PAPER

Fast and stable redox reactions of MnO$_2$/CNT hybrid electrodes for dynamically stretchable pseudocapacitors†

Taoli Gu and Bingqing Wei*

Pseudocapacitors, which are energy storage devices that take advantage of redox reactions to store electricity, have a different charge storage mechanism compared to lithium-ion batteries (LIBs) and electric double-layer capacitors (EDLCs), and they could realize further gains if they were used as stretchable power sources. The realization of dynamically stretchable pseudocapacitors and understanding of the underlying fundamentals of their mechanical–electrochemical relationship have become indispensable. We report herein the electrochemical performance of dynamically stretchable pseudocapacitors using buckled MnO$_2$/CNT hybrid electrodes. The extremely small relaxation time constant of less than 0.15 s indicates a fast redox reaction at the MnO$_2$/CNT hybrid electrodes, securing a stable electrochemical performance for the dynamically stretchable pseudocapacitors. This finding and the fundamental understanding gained from the pseudo-capacitive behavior coupled with mechanical deformation under a dynamic stretching mode would provide guidance to further improve their overall performance including a higher power density than LIBs, a higher energy density than EDLCs, and a long-life cycling stability. Most importantly, these results will potentially accelerate the applications of stretchable pseudocapacitors for flexible and biomedical electronics.

Introduction

Flexible/stretchable electronics can be bent, twisted and even stretched, and they represent the emerging trend towards next-generation wearable and bio-implantable electronic devices. Stretchable power sources are the key components for the fabrication of complete and independent stretchable electronic systems. To date, stretchable energy storage devices including stretchable electric double-layer capacitors (EDLCs) and stretchable lithium ion batteries (LIBs) have been reported to show excellent mechanical and electrochemical properties.[1–4] However, there is an urgent need to design and develop a stretchable power source with a higher power density than LIBs and a higher energy density than EDLCs. In light of this, the development of stretchable pseudocapacitors has become indispensable.

Pseudocapacitors normally combine non-faradaic electrostatic charge storage processes from carbon based materials with redox reactions based on metal oxides and/or conductive polymers to achieve a higher specific capacitance while at the same time, maintaining their quick charge–discharge feature. A significant number of hybrid electrodes, such as carbon nanotube (CNT)/ruthenium(IV) oxide (RuO$_2$),[5] CNT/manganese dioxide (MnO$_2$),[6] graphene/MnO$_2$,[7] and graphene/polyaniline (PANI)[8] have been investigated as flexible pseudocapacitors, however, fully stretchable pseudocapacitors are relatively underdeveloped. Hu *et al.*[9] deposited nanoparticles on CNT films as stretchable electrodes for pseudocapacitors, but no electrochemical testing of the stretched states was performed. Another work on stretchable pseudocapacitors was reported based on conductive polymer (polypyrrole, PPy) coated textiles.[10] PPy coated nylon "lycra" fabric delivered a much higher capacitance than the stretchable CNT based electrodes,[1–3] but with poor cycling stability; the sample degraded to have less than 12.5% of the initial capacitance within 500 charge–discharge cycles. Since the conductive polymer (PPy) was directly pasted onto the textile to form a stretchable electrode, a significant decrease in the electric conductivity occurred during repeated mechanical stretching–releasing due to the gradual loss in electrical contacts between PPy and the textile material. It is therefore equivalently important to increase both the specific capacitance and the interface stability for stretchable pseudocapacitors. Unlike the stretchable EDLCs, which are based solely on a buckled CNT film,[1–3] the strong bonding between the active materials (*i.e.* MnO$_2$ in this research) and

Department of Mechanical Engineering, University of Delaware, Newark, DE 19716, USA. E-mail: weib@udel.edu

the CNT substrates in pseudocapacitors is another very critical requirement.

It is therefore crucial to explore building a stretchable pseudocapacitor system and to understand its fundamental characteristics in order to meet the stringent requirements imposed by the various applications of stretchable electronics. For example, it is unclear whether a redox reaction of a pseudocapacitor is fast enough to maintain its electrochemical stability under intense and dynamic mechanical stretching and bending. How would the dynamic stretching/releasing affect the electrochemical properties of the stretchable pseudocapacitors since the charge storage mechanism of pseudocapacitors is completely different from that of EDLCs?

Herein, we demonstrate dynamically stretchable pseudocapacitors (DSPs) based on MnO_2/CNT hybrid electrodes for the first time, with simultaneous monitoring of the mechanical and electrochemical behaviors at different charge–discharge current densities and mechanical strain rates. Most importantly, the redox reaction process of the typically pseudocapacitive material MnO_2 has been found to be extremely fast owing to the strongly bonded, inherently superior conductive and porous CNT films,[11] which facilitate the charge transfer of the redox processes of the stretchable pseudocapacitors. Because of this, the pseudo-capacitive stability would not be affected even under a dynamic mechanical deformation. This understanding would provide important guidelines for the design and development of highly stable and stretchable pseudocapacitor devices.

Experimental

Dynamically stretchable pseudocapacitor (DSP) assembly

First, CNT films were prepared using a modified chemical vapor deposition method according to previously published work.[11] In brief, the precursor, a mixture of ferrocene and sulfur (atomic ratio Fe : S = 1 : 10, both from Sigma Aldrich), was heated to 1150 °C in a tube furnace with a mixed gas flow of Ar (1500 mL min^{-1}) and H_2 (150 mL min^{-1}). After a 75 min reaction, the as-obtained unpurified CNT films were transferred into a ceramic cubicle to be heat-treated at 430 °C in air for 30 min. When the furnace was cooled to room temperature, the CNT films were immersed in a concentrated HCl (37% by volume percent) solution for 72 h to remove the Fe_2O_3 from the oxidation of Fe catalysts during the heat treatment. The films were then rinsed with deionized (DI) water until the pH was neutral.

The MnO_2/CNT hybrid film electrodes were then prepared by modified precipitation.[12] Briefly, the purified CNT film was immersed in ethanol, while a 0.1 M $KMnO_4$ aqueous solution was added drop-wise. Thin layers of nanostructured MnO_2 were deposited on the surface of the CNT bundles with different precipitation times. The resulting MnO_2/CNT electrodes were rinsed excessively in deionized water and ethanol and finally dried at room temperature for 24 h.

The procedure to prepare the buckled MnO_2/CNT electrode is as follows: a custom-made two-way movable stage was utilized to pre-stretch a polydimethylsiloxane (PDMS) substrate; the pre-strained PDMS was subjected to UV light for 1 min to activate the surface functional groups to facilitate the strong bonding with the MnO_2/CNT film. Next, the freestanding MnO_2/CNT film was attached and secured to the PDMS substrate. Finally, the PDMS was released to its original length to form the "wavy" structure of the buckled MnO_2/CNT film. An elastomeric polyurethane separator was prepared by electrospinning.[2] Finally, these components were assembled together and 1 M $TEABF_4$/PC electrolyte was injected into the cell package.

Characterization

The morphology and structure of the MnO_2/CNT and CNT films were characterized by means of scanning electron microscopy (3 kV, JEOL JSM-7400F). The masses of the active materials were acquired using a micro/ultra-micro balance (Mettler Toledo XP6) with 0.001 mg accuracy. The stretchable cells were assembled in an argon-filled glove box (MBraun Unilab). The galvanostatic discharge–charge tests were carried out on four-channel battery testing equipment (Arbin Instrument, Ltd). Electrochemical impedance spectroscopy was performed on a PARSTAT 2273 potentiostat/galvanostat (Princeton Applied Research) with 10 mV amplitude of AC signals from 100 kHz to 10 mHz. Cyclic voltammetry measurements were also obtained using the electrochemical workstation (Princeton Applied Research) in the scan range of −1.5 V to 1.5 V. The electrochemical measurements were performed while the DSP was being stretched and released between 0% (when the MnO_2/CNT film was buckled) and 33.33% strain (when the MnO_2/CNT film was almost flattened). The strain rates were set at 1.5% strain per s, 3% strain per s and 6% strain per s, respectively. The DSR test results reveal the real performance of the stretchable energy storage device.

Calculations

The specific capacitance of the MnO_2/CNT electrodes was calculated based on the total mass of the electrode and was calculated from the slope of the discharge capacitance. The energy and power densities were calculated by conducting galvanostatic charge–discharge cycling with different constant current densities ranging from 100 mA g^{-1} to 100 A g^{-1}. The frequency dependence of the real and imaginary parts (C' and C'') of the electrochemical capacitance was obtained from the electrochemical impedance spectroscopy measurements.

Results and discussion

Fig. 1a presents a typical scanning electron microscope (SEM) image of the pristine CNT films synthesized using a chemical vapor deposition method.[11] It can be seen that the single-walled CNT bundles entangle each other to form porous structures consisting of mesopores and macropores, which provide
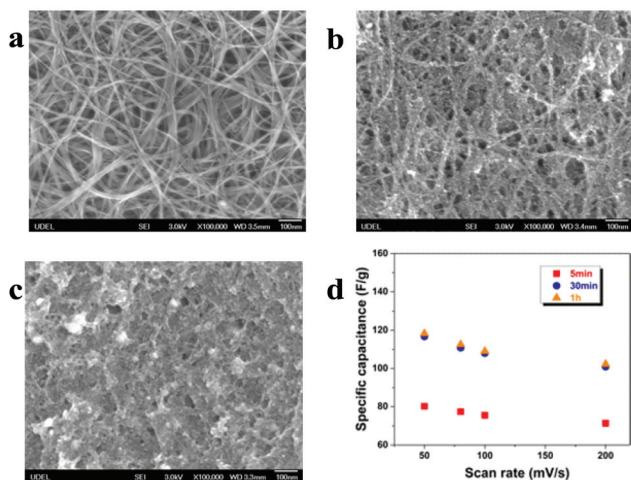
Fig. 1 (a) Pristine CNT films as synthesized before coating with the MnO_2 layers. (b) Buckled MnO_2/CNT electrode as-synthesized with 30 min precipitation time. (c) Buckled MnO_2/CNT electrode after 10 000 charge–discharge cycles and 24 300 simultaneous stretching–releasing cycles. (d) Scan rate dependence of the specific capacitance based on the total mass of the MnO_2/CNT electrodes with respect to the different precipitation times (5 min, 30 min, and 1 hour as examples).

superior electrical conductivity, large electrode/electrolyte interfaces and easy pathways for electrolyte ions, thus facilitating the charge transfer by reducing the electronic and ionic diffusion resistances. Fig. 1b illustrates the morphology of the MnO_2/CNT hybrid films as the stretchable pseudocapacitor electrodes. The MnO_2 nanoparticles are uniformly deposited on the surfaces of the CNT bundles to form a thin MnO_2 layer by employing a facile precipitation method.[12]

After many galvanostatic charge–discharge (GCD) cycles (10 000 cycles) under dynamic mechanical stretching–releasing (24 300 cycles) at 6% strain per s, the surface morphology was examined with SEM (Fig. 1c). There are no noticeable detachments of the MnO_2 nanoparticles from the CNT bundles but there are some residues from the electrolyte salt, as compared with the surface before the cycling test in Fig. 1b. The MnO_2 thin layers retain similar morphologies after the long charge–discharge and stretching–releasing cycles, indicating very strong bonding between the MnO_2 nanoparticles and the CNT bundles. This behaviour can be attributed to the interconnected porous and fabric-like structures of the CNT film as well as the surface functional groups introduced during the post-treatment of the CNT films that significantly enhance the bonding between the active material (MnO_2) and the CNT bundles. The merit of the thin MnO_2 layer grown on the CNT bundles is the shortening of the diffusion path for the electrolyte ions during the fast charge–discharge processes, thus ensuring its full contribution to the pseudo-capacitive performance, and significantly improving the specific capacitance of the DSPs. More important and significant for DSPs, however, the thin MnO_2 layer attached on the CNT surfaces can withstand the

intense stress during mechanical stretching and releasing, which is critical in determining whether the hybrid materials could be a good candidate for stretchable/flexible energy storage devices. As shown in Fig. 1d, the optimized loading (20% MnO_2 mass ratio) in our experiments was obtained with a 30 min precipitation time. The DSPs were characterized using the optimized loading for all MnO_2/CNT electrode preparations in the following discussion.

Fig. 2a illustrates the assembly of DSPs, including two PDMS packages embedded with two buckled MnO_2/CNT electrodes and an elastomeric separator. The as-fabricated pseudocapacitors are highly deformable and can be dynamically stretched and released without destroying their structural integrity (as in the schematic in Fig. 2b). The electrochemical characterization of the DSPs under GCD cycling was examined at a high current density of 10 A g^{-1}, exhibiting the high power capability of the hybrid MnO_2/CNT electrodes. The symmetry profile of the charge and discharge curve also reveals the good
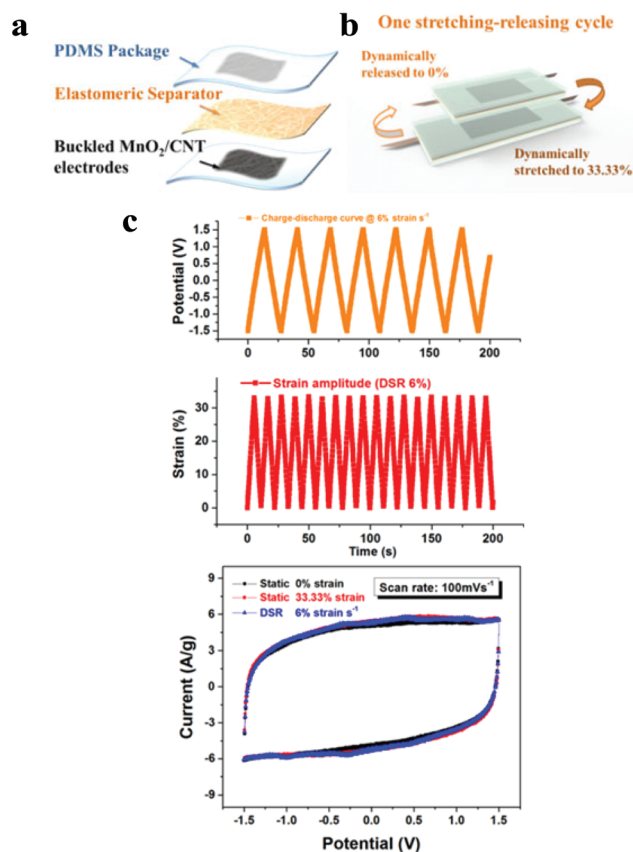

Fig. 2 (a) Schematic of the main components of the dynamically stretchable pseudocapacitors (DSPs). (b) Schematic of one mechanical stretching–releasing cycle: the reversible dynamic stretching and releasing between 0 and 33.33% applied strains. (c) Upper: galvanostatic charge–discharge curve at a current density of 10 A g^{-1} under dynamic stretching–releasing (DSR) at a strain rate of 6% strain per s. Middle: the simultaneous dynamic mechanical strain amplitude variation between 0 and 33.33% strain at 6% strain per s. Bottom: cyclic voltammograms (CVs) of the DSPs measured at a scan rate of 100 mV s^{-1}.

capacitive characteristics of the DSPs and in particular, the inherently fast surface redox behaviour of the MnO_2/CNT pseudo-capacitive materials. Similar electrochemical behaviour has also been observed at other strain rates, at 3% strain per s and 1.5% strain per s (Fig. S4a†). Although the mechanical stretching–releasing modes are different for each state, the charge–discharge curves at different strain rates almost overlap, proving that the pseudo-capacitive behaviour is stable, reversible and independent of the strain rate.

Dynamic cyclic voltammetry (CV) is another important electrochemical–mechanical coupling test used to evaluate the electrochemical stability of the stretchable pseudocapacitors. CVs were tested under dynamic stretching–releasing (DSR) and in a static stretched state with respect to the minimum strain (0%) and maximum strain (33.33%). As exemplarily shown in Fig. 2c, under the DSR mode with a high strain rate of 6% strain per s (11.11 s for one mechanical stretching–releasing cycle, which is defined to be a dynamic stretching from 0 to 33.33% applied strain and then back to 0% strain), the reproducible and stable capacitive behaviour of the DSPs at a scan rate of 100 mV s^{-1} reveals an uncoupling effect between the mechanical strain and the electrochemical performance. The changes in the electrochemical performance of the fabricated pseudocapacitor seem to be subtle under the dynamic mechanical stretching–releasing processes at the high strain rate of 6% strain per s. In addition, it is interesting to note that the CV curve under the DSR mode shifts between the static CV curves of the maximum (33.33% fixed static strain) and the minimum (0% fixed static strain). Accordingly, the pseudo-capacitance under the different testing conditions also show similar results; i.e. at various DSR strain rates (from 1.5 to 6% strain per s) and different scan rates (from 100 to 1000 mV s^{-1}), the CV curves for the DSR cases shift between the CV curves for 0 to 33.33% static strain (Fig. S2a–c and S3a–d†). It is worth mentioning that the CV curves at the extremely high scan rate of 1000 mV s^{-1} also maintain a typical rectangular shape, analogous to the non-faradaic processes for stretchable EDLCs,[2] indicating a highly reversible and fast faradaic reaction of MnO_2 due to the improved conductivity from the interconnected CNT film. These results further prove the excellent pseudo-capacitive stability of DSPs under stretching–releasing modes with high scan rates.

To explore the long cycle stability of the DSPs, 10 000 GCD cycles were carried out at a current density of 10 A g^{-1}. As shown in Fig. 3a, the capacitance retention with the 30 min-precipitation hybrid MnO_2/CNT electrodes was maintained at 97.30%, 97.64% and 98.50% at the strain rates of 1.5, 3 and 6% strain per s, respectively. However, the capacitance retention for the hybrid MnO_2/CNT electrodes with 1 hour precipitation dropped to 76.15% and 59% after 10 000 GCD cycles at the strain rates of 3% and 6%, respectively (Fig. S1a and b†), a poor cycling stability compared to the 5 min and 30 min hybrid MnO_2/CNT electrodes. It further confirms that the 30 min-precipitation hybrid MnO_2/CNT electrodes provide the best overall performance and a thicker MnO_2 layer would result in poor contact and bonding with the CNT films.
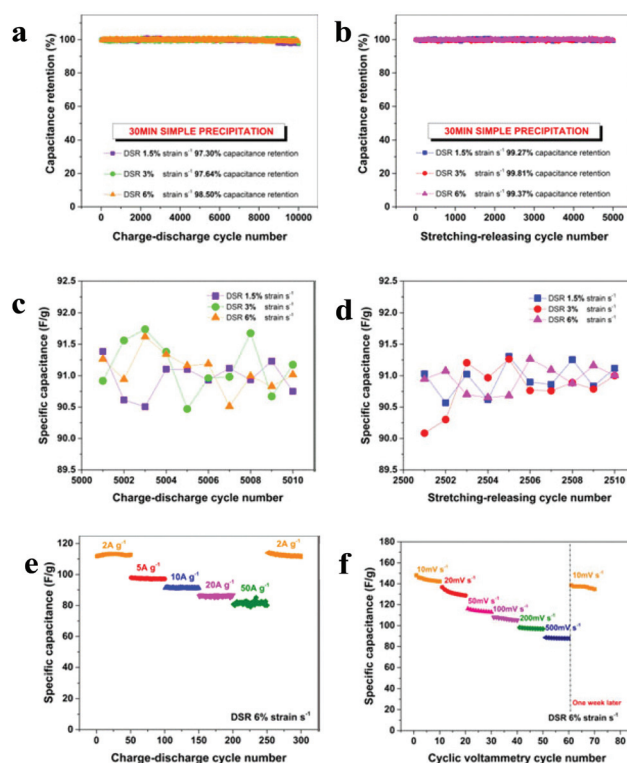

Fig. 3 Simultaneous charge–discharge cycling and applied DSR at the strain rates of 1.5, 3 and 6% strain per s. The DSP with a 30 min precipitation time shows excellent cycling stability for (a) 10 000 electrochemical charge–discharge cycles and (b) 5000 mechanical stretching–releasing cycles. Less than 1.5 F g^{-1} capacitance fluctuation is observed from the zoomed-in charge–discharge cycles from 5001 to 5010 (c) and the stretching–releasing cycles from 2501 to 2510 (d). Cycling stability at (e) consecutively varied current densities and (f) with consecutively varied cyclic scan rates at the strain rate of 6% strain per s.

For stretchable energy storage devices, the attainable mechanical stretching–releasing cycles, which reveal their durability for practical applications, are also very critical in addition to evaluating their GCD cycling stability. The DSPs were tested for 5000 DSR cycles with different strain rates of 1.5, 3 and 6% strain per s (the time for one stretching–releasing cycle is 44.44, 22.22 and 11.11 s, respectively) and at a constant current density of 10 A g^{-1}. Fig. 3b shows that the capacitance retention is extremely high at all strain rates, where the capacitance fades by less than 1%, further proving the excellent durability of the pseudocapacitors from the mechanical viewpoint.

In order to illustrate the detailed capacitance variation under both charge–discharge and the stretching–releasing cycles, the dynamic behavior at different strain rates are enlarged and depicted in Fig. 3c and d. The capacitance fluctuates from 90 to 92 F g^{-1} and the variation is less than 1.5 F g^{-1}, which is within 2.5% of the capacitance. This extremely stable capacitive behavior at various strain rates indicates that there is no significant effect from the mechanical stretching–releasing on the charge–discharge performance of the pseudocapacitor cell, proving that the pseudocapacitors can be reversibly charged and discharged under dynamic stretching.

In order to investigate the rate capability of DSPs, the cycling performance at progressively increasing current densities was recorded at the strain rate of 6% strain per s and is shown in Fig. 3e. Even when experiencing sudden changes of current density, the stretchable pseudocapacitor exhibits a very stable capacitance at each current density (50 cycles at each current density) from 2 to 50 A g^{-1}. After 250 continuous cycles at varied current densities, the current density was turned back to 2 A g^{-1} and ~99.9% of the initial capacitance (~112 F g^{-1}) could still be recovered.

To further highlight the stability of the stretchable structure design of the DSPs, programmed CV testing was also recorded. The DSP was initially subjected to 10 continuous cycles at 10 mV s^{-1} and was then measured at 20, 50, 100, 200, and 500 mV s^{-1}, successively, at the strain rate of 6% strain per s. The stepwise testing reveals that the cell can remain electrochemically stable even after sudden scan rate changes and continues to be stable under the intense and dynamic mechanical loading. The specific capacitance of the MnO$_2$/CNT cell decreases to 100 F g^{-1} from ~119 F g^{-1} as the scan rate increases from 50 to 200 mV s^{-1}, representing only a 16% decrease compared with the value at the scan rate of 50 mV s^{-1}. This result indicates the excellent capacitive behaviour and high-rate capability of DSPs. Furthermore, upon switching the scan rate back to 10 mV s^{-1}, the specific capacitance of MnO$_2$/CNT was able to be recovered fully, demonstrating the excellent capacitance retention of the DSPs. It is also meaningful to point out that in order to examine the endurance capabilities of the cell, we purposely suspended the CV test for one week, and resumed the test for another 10 cycles under the same scan rate of 10 mV s^{-1}. There is only a slight capacitance loss, thus showing excellent capacitance durability.

Pseudo-capacitance is expected to be much higher than the EDLC-capacitance because pseudo-capacitive materials take advantage of relatively slow redox reactions. However, the redox kinetics of the hybrid MnO$_2$/CNT system for stretchable pseudocapacitors are unclear. The principal objective of the electrochemical impedance spectroscopy (EIS) measurements was to gain insights into how fast the pseudo-capacitive behaviour could be for the MnO$_2$/CNT system in stretchable modes and its coupling effects with the dynamic mechanical strain rate. Fig. 4a shows the Nyquist plots in the frequency range from 100 kHz to 10 mHz measured at equilibrium open circuit potential at different strain rates from 0.15% strain per s to 6% strain per s with repeated dynamic stretching and releasing. We introduced here an extremely slow strain rate with 0.15% strain per s (444.4 s for one mechanical stretching–releasing cycle) in order to create a mechanically stable environment to ensure that the mechanical cycle time is sufficiently long for the redox reaction of the stretchable pseudocapacitors. The Nyquist plots can be represented by a modified Randles circuit with a set of resistors and capacitors in series and parallel as shown in Fig. 4b. The first intersection point on the real axis of the Nyquist plot in the high-frequency region provides the value of the series resistance R_s. The charge transfer resistance R_{ct} is the second intersection point of the semicircle on the
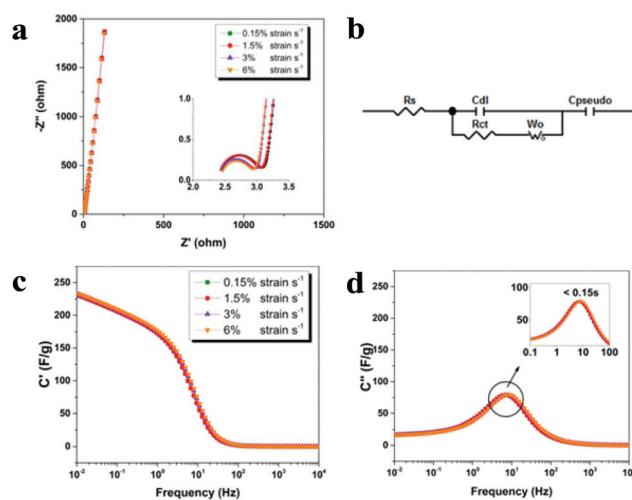

Fig. 4 (a) Electrochemical impedance spectroscopy measurements on the dynamically stretchable pseudocapacitors at different strain rates with repeated stretching and releasing in the frequency range from 100 kHz to 10 mHz. Inset: the enlarged high frequency region of the Nyquist Plots. (b) Modified Randles equivalent circuit representing the circuit elements in the Nyquist plots. The equivalent circuit is used to fit the Nyquist plots using the software ZVIEW. (c) Bode plots of the real specific capacitance. (d) Bode plots of the imaginary specific capacitance, related to the relaxation time constant. Both are calculated from the EIS data for the DSPs at 0.15, 1.5, 3, and 6% strain per s. C′ and C″ are the real specific capacitance and imaginary specific capacitance, respectively.

real axis which is mainly derived from the resistance between the electrode and the electrolyte. The double layer capacitance C_{dl} is connected in parallel to R_{ct}. The semicircle proves that there are charge transfer processes for the MnO$_2$/CNT pseudocapacitors. After the semicircle, the Nyquist plots show a long tail in the low-frequency region pertaining to the diffusion of ions into the bulk of the electrode. The transition from the mid-frequency to the low-frequency tail is represented by the Warburg diffusion element, W_o. Faradaic capacitance arises from the contribution of MnO$_2$ and is represented as C_{pseudo}. At high frequencies, the capacitor impedance becomes much smaller and the system resistance is dominated by the resistors and polarization impedances. At low frequencies, an ideal polarizable capacitance would give a straight line with large angles with respect to Z' or almost parallel to Z''.

As shown in Fig. 4a, the low frequency straight lines are almost vertical, indicating good capacitive behaviour. Both R_s and R_{ct} are very small at all strain rates, as shown by the high-frequency semicircle of the pseudocapacitors in the inset of Fig. 4a, which emphasizes the excellent electric pathways of the CNT and the fast redox reactions of MnO$_2$ in the pseudo-capacitive material resulting from the MnO$_2$/CNT hybrid structure.

All of the equivalent circuit-fitting results were performed using the EIS data fitting program ZVIEW and presented in Table 1. It is observed that the values of all of the fitting parameters are almost stable with different strain rates. However, it is interesting to notice that the strain rate slightly affects the

Table 1 Equivalent circuit parameters obtained from the curve fitting results

Fitting parameter	R_s (Ω)	C_{dl} (F g^{-1})	R_{ct} (Ω)	W_o (Ω)	C_{pseudo} (F g^{-1})
0.15% strain per s	2.45	0.12	0.57	0.48	106.35
1.5% strain per s	2.44	0.12	0.57	0.48	106.76
3% strain per s	2.44	0.14	0.48	0.45	106.94
6% strain per s	2.47	0.16	0.43	0.44	109.53

pseudocapacitive performance, with a small decrease of R_{ct} to 0.43 ohms at DSR 6% strain per s from 0.57 ohms at DSR 0.15% strain per s, indicating an improved electrode/electrolyte interface at a relatively high strain rate. This could possibly be attributed to better wetting of the MnO$_2$/CNT surface by the increased strain rate, which gives easier access to the electrolyte ions to permeate into the electrode materials. We express it as the mechanical activation for stretchable/flexible energy storage devices: a faster dynamic stretching and releasing leads to an increase in the values of C_{dl} and C_{pseudo}; however, the increments are very small. Compared to EDLCs, a pseudocapacitor with the buckled MnO$_2$/CNT electrodes has two components to contribute to the mass capacitance, EDLC capacitance (C_{dl}) and the pseudocapacitance (C_{pseudo}). As shown in Table 1, it is obvious that the DSP system is pseudocapacitance dominant and the pseudo-capacitive stability could ensure the stable performance of the DSPs.

The relaxation time constant τ_0 ($\tau_0 = f_0^{-1}$) is a quantitative measure of how fast a capacitor device can be charged and discharged reversibly and is of practical importance in determining the rate at which the electrical response of a capacitor device can take place. The relaxation time constant from Fig. 4d in the frequency-dependent imaginary capacitance analysis quantitatively reveals its performance and these results give valuable insight into the role of dynamic strain variation in the frequency response of the DSPs. In Table 2 and Fig. 4d, the relaxation time constant is less than 0.15 s at all strain rates under the dynamic stretching and releasing for the DSPs, much shorter than reported values for planar activated carbon based microsupercapacitors[13] (∼0.7 s) and multi-wall nanotube based supercapacitors[14] (∼0.7 s). The extremely short relaxation time constant could be attributed to the excellent conductivity of the CNT network, which facilitates the redox reaction of MnO$_2$ and leads to rapid pseudo-capacitive behaviour. Although the mobility of the ions in the organic electrolyte is slower than that of the ions in the aqueous electrolyte

due to the larger viscosity and the larger ion size, the relatively weak chemisorption between the MnO$_2$ and electrolyte interface leads to fast adsorption/desorption and thus an extremely small relaxation time constant, which further confirms that the redox reaction would be initiated from the surface layer of the manganese oxides in contact with the electrolyte. Compared to the mechanical stretching–releasing cyclic time (τ'), in which the DSP accomplishes one mechanical stretching–releasing cycle, τ_0 is extremely short, at least two magnitudes shorter (Table 2). This extremely short relaxation time constant τ_0 at all strain rates for DSPs strongly suggests that the pseudocapacitors built with the buckled MnO$_2$/CNT electrodes possess enormous potential for stable and instantaneous delivery of ultrahigh power and energy under rapid mechanical deformation.

Conclusions

In conclusion, the electrochemical stability of dynamically stretchable pseudocapacitors based on the buckled MnO$_2$/CNT electrodes was systematically studied at different strain rates during stretching for the first time. We have successfully demonstrated the excellent pseudo-capacitive stability of the DSPs under both electrochemical charge–discharge cycles and mechanical stretching and releasing cycles. The long cycle GCD measurements also showed excellent stability in capacitance from both electrochemical and mechanical viewpoints. The extremely small relaxation time constants fundamentally explained that repeated stretching and releasing at the applied strain rates will not affect the stable performance of DSPs. All of these findings are expected to highlight a broad area of stretchable energy storage devices including DSPs.

Acknowledgements

Notes and references

1 C. Yu, C. Masarapu, J. Rong, B. Wei and H. Jiang, *Adv. Mater.*, 2009, **21**, 4793–4797.
2 X. Li, T. Gu and B. Wei, *Nano Lett.*, 2012, **12**, 6366–6371.
3 Z. Niu, H. Dong, B. Zhu, J. Li, H. H. Hng, W. Zhou, X. Chen and S. Xie, *Adv. Mater.*, 2013, **25**, 1058–1064.
4 S. Xu, Y. Zhang, J. Cho, J. Lee, X. Huang, L. Jia, J. a. Fan, Y. Su, J. Su, H. Zhang, H. Cheng, B. Lu, C. Yu, C. Chuang, T.-I. Kim, T. Song, K. Shigeta, S. Kang, C. Dagdeviren, I. Petrov, P. V. Braun, Y. Huang, U. Paik and J. a. Rogers, *Nat. Commun.*, 2013, **4**, 1543.
5 P. Chen, H. Chen, J. Qiu and C. Zhou, *Nano Res.*, 2010, **3**, 594–603.

Table 2 Comparison of the relaxation time constant (τ_0) and stretching–releasing cycle time (τ') at different strain rates

Strain rate	τ_0 (s)	τ' (s)
0.15% strain per s	0.148	444.4
1.5% strain per s	0.148	44.44
3% strain per s	0.126	22.22
6% strain per s	0.126	11.11

6 J. Kim, K. H. Lee, L. J. Overzet and G. S. Lee, *Nano Lett.*, 2011, **11**, 2611–2617.

7 Y. He, W. Chen, X. Li, Z. Zhang, J. Fu, C. Zhao and E. Xie, *ACS Nano*, 2013, **7**, 174–182.

8 K. Zhang, L. L. Zhang, X. S. Zhao and J. Wu, *Chem. Mater.*, 2010, **22**, 1392–1401.

9 L. Hu, M. Pasta, F. La Mantia, L. Cui, S. Jeong, H. D. Deshazer, J. W. Choi, S. M. Han and Y. Cui, *Nano Lett.*, 2010, **10**, 708–714.

10 B. Yue, C. Wang, X. Ding and G. G. Wallace, *Electrochim. Acta*, 2012, **68**, 18–24.

11 H. Zhu and B. Wei, *Chem. Commun.*, 2007, 3042–3044.

12 X. Li and B. Wei, *Nano Energy*, 2012, **1**, 479–487.

13 D. Pech, M. Brunet, H. Durou, P. Huang, V. Mochalin, Y. Gogotsi, P.-L. Taberna and P. Simon, *Nat. Nanotechnol.*, 2010, **5**, 651–654.

14 C. Portet, G. Yushin and Y. Gogotsi, *Carbon*, 2007, **45**, 2511–2518.